P3.4

DIFFERENCES BETWEEN THE NORTH PACIFIC AND ENSO MODES

Soon-Il An and Bin Wang
International Pacific Research Center, University of Hawaii at Manoa, Honolulu, Hawaii

1. INTRODUCTION

The low-frequency mid-latitude atmospheric circulation anomalies are usually characterized by the Pacific-North American (PNA) and North Atlantic Patterns (Wallace and Gutzler 1981). The PNA has been interpreted as forced by El Nino-Southern Oscillation (ENSO) via atmospheric teleconnection (e.g., Horel and Wallace 1981). On the contrary, many studies showed that the internal atmospheric dynamical processes in the midlatitude atmosphere could generate a PNA-like pattern through the barotropic and baroclinic instability (Simmons et al. 1983). Recently, Strauss and Shukla (2002) analyzed winter ensemble GCM simulation, and concluded that the PNA pattern is characteristic of internal dynamics that is distinct from the ENSO forced midlatitude circulation pattern. Zhang et al. (1996) separated the intrinsic mid-latitude air-sea coupled mode in the North Pacific (hereafter the North Pacific (NP) Mode) from the ENSO induced mid-latitude coupled pattern (hereafter ENSO Mode). So far, it is uncertain whether those two modes are really distinct not only statistically but also physically in the observational point of view.

In this study, we try to identify the coupled patterns of variability between mid-troposphere geopotential height and SST anomalies over the tropical and North Pacific using the conditional maximum covariance analysis (CMCA) (An 2003). Our intention is to derive a coupled North Pacific pattern that is statistically unrelated to ENSO and then compare its behavior with the ENSO-forced mode.

2. DATA AND METHODOLOGY

The datasets used in this study are monthly-mean North Pacific 500-hPa geopotential height (hereafter, GPH) obtained from NCEP reanalysis data (Kalnay et al. 1996), and Pacific SST obtained from the Reynolds (Reynolds and Smith 1994). Each data set covers the period from 1950 to 1999.

To obtain coherent patterns between GPH and SST and to remove unwanted signals, we adopt CMCA (An 2003). The method is following: Consider two geophysical variables, $\xi^*(\vec{x},t)$ and $\psi^*(\vec{x},t)$ and a constraint time series $Z(t)$. Now, we construct two new variables $\xi(\vec{x},t)$ and $\psi(\vec{x},t)$, by removing the portions of the signals in ξ^* and ψ^* that are covariant with $Z(t)$;

$\xi = \xi^* - Z \times \mathrm{COV}(\xi^*,Z)/\mathrm{VAR}(Z)$ and

$\psi = \psi^* - Z \times \mathrm{COV}(\psi^*,Z)/\mathrm{VAR}(Z)$, (1)

where COV(x,y) denotes the temporal covariance between variables x and y, and VAR(z) denotes the variance of z. The ξ and ψ are no more correlated with Z. By applying the maximum covariance analysis (MCA) (a.k.a. SVD, Wallace et al. 1992) to these newly defined variables, we can identify pairs of spatial patterns that explain as much as possible of the mean-squared temporal covariance between two variables. Thus, Conditional MCA, CMCA(ξ^*,ψ^*;Z) provides coupled patterns between ξ and ψ, in which the signals related to Z has been excluded. Here, Z will be referred to as the secondary predictor.

3. COHERENT SST AND 500-HPA GEOPOTENTIAL PATTERNS ASSOCIATED WITH NP AND ENSO MODES

The CMCA method is applied to the 500-hPa GPH and SST anomalies (Fig. 1). In this calculation, the Nino-3 index (5°S-5°N, 150°-90°W) was used as the secondary predictor. The GPH pattern tends to be zonally elongated, and its center is located at 45°N, 170°W. The area of negative GPH anomalies matches that of the negative SST anomalies. The ENSO-like pattern in the tropical Pacific disappears. The ENSO signal in their corresponding expansion coefficients is also not detectable. In other words, this mode has little connection with the tropical SST anomalies. This mode resembles 'North Pacific mode' (Zhang et al. 1996).

The CMCA method is again applied to GPH and SST anomalies, in which the expansion coefficients associated with the SST pattern of the NP mode is used as the secondary predictor (Fig. 2). Clearly, the SST pattern in the tropical Pacific resembles ENSO signature. In addition, every peak appeared in the expansion coefficients corresponds to El Nino/La Nina events (hereafter, this mode will be referred as 'ENSO mode'). The GPH anomalies associated with the ENSO mode show some subtle difference with that of the NP mode. The negative center of the GPH anomalies shifts slightly southeastward with its axis tilting toward the southeast (Fig. 2a). There is a weak ridge occurring near Japan, which is absent in the NP mode. Along this ridge, positive SST anomalies are found. In the NP mode, the SST anomalies in this region are negative. Overall, the NP and ENSO modes show a different feature in their spatial and temporal behaviors.

4. TEMPORAL CHARACTERISTICS OF NP AND ENSO MODES

The lagged correlation between the expansion coefficients of the NP mode for SST and those for GPH (hereafter, the former refers to NP-SST time series and the latter refers to NP-GPH time series) is

*Corresponding author address: Soon-Il An, Univ. of Hawaii, IPRC, Honolulu, HI 96822; e-mail: sian@hawaii.edu.

calculated (not shown). When the NP-GPH leads NP-SST, the correlation is significant over 99% confidence level from lag 0 to 4 months. The maximum positive correlation appears at one-month positive lag that may be attributed to the delayed oceanic thermal response to the atmospheric forcing. The slow decrease of the correlation after one month may be related to relatively slow damping of the ocean temperature. When NP-SST leads NP-GPH, the correlation is insignificant. In contrast, for the ENSO mode the maximum correlation between ENSO-SST and ENSO-GPH time series is obtained when SST leads the GPH.

We calculate the autocorrelation of NP-SST and ENSO-SST time series for each calendar month to examine the persistence (Fig. 3). The NP mode has the most significant persistence in FEB-APR with lead times of 3 months, while it has the least persistence in JUL-SEP (Fig. 3a). On the other hand, the ENSO mode starting in JAN-APR has the least persistence and that in JUN-AUG has the longest persistence (Fig. 3b).

5. UPPER AND LOWER ATMOSPHERIC CIRCULATION ANOMALIES, AND TRANSIENT ACTIVITIES

The linear regression maps of 200- and 1000-hPa wind vectors, and transient activities against NP-SST time series and ENSO-SST time series are calculated (not shown here). Both upper and lower level wind patterns associated with the NP mode are basically confined to the North Pacific, whereas those associated with the ENSO mode are confined in the tropical Pacific. The upper-tropospheric jet stream associated with the NP and ENSO modes intensifies, respectively, over the central North Pacific and the subtropical northeastern Pacific, and in each jet exit region, the transient activities are intensified.

6. IS THERE A LINKAGE BETWEEN NP AND ENSO MODES?

To resolve the dilemma of a significant simultaneous correlation between NP-GPH time series and ENSO-GPH time series, we suppress the high frequency variability in both NP-GPH and ENSO-GPH time series. The idea is that the ocean tends to response to integrated atmospheric stochastic forcing such as mid-latitude weather, which results in “reddened” noise with increased power at low frequencies and decreased power at high frequencies (e.g., Frankignoul and Hasselmann 1977). We adopt a simple AR-type model,

$$P_n = \alpha P_{n-1} + \xi_n \qquad (2)$$

where P is a predictand, ξ is a predictor, α is a reddening factor, and n denotes time (in months).

First, we take the normalized NP-GPH time series as ξ. Using Eq. (2), we calculate P for a given ξ, where P can be considered as a predicted SST anomaly of the NP mode. Thus, P becomes the reddened quantities of NP-GPH time series. We perform the sensitivity test on the reddening factor α (between 0 and 1) for the same ξ. The correlation between the reddened quantities and NP-SST time series is shown in Fig. 4 (solid line). The increase of the reddening factor results in an increase of the correlation up to 0.77, which is much higher than the original calculation (that when α=0). On the other hand, the correlation between the reddened quantities and ENSO-GPH time series decreases gradually to zero as α approaches 1. In other words, as the high-frequency fluctuation of GPH decreases (corresponding to increasing α), the correlation between NP-GPH time series and ENSO-GPH time series becomes meaningless. It indicates that the high correlation between NP-GPH and ENSO-GPH is due to high-frequency fluctuations.

Secondly, we have reddened ENSO-GPH time series (here, ξ becomes the normalized ENSO-GPH time series), and calculate the correlation between the reddened ENSO-GPH time series and NP-SST time series. As shown in Fig. 4 (dash-dotted-line), as the reddening factor increases, the correlation also increases. However, its maximum value is below 0.3, which is far less than the correlation between NP-GPH and NP-SST time series. In other word, the reddening of ENSO-GPH time-series cannot improve the relationship between ENSO-GPH and NP-SST, indicating that the NP mode is clearly different from ENSO mode. Thus, the significant simultaneous correlation between NP-GPH and ENSO-GPH time series must result from the high-frequency signals that are unrelated to the corresponding SST variation.

7. SUMMARY

The coherent patterns between the tropical and North Pacific SST and the North Pacific 500-hPa geopotential height anomalies are identified as two leading modes: an intrinsic midlatitude mode, the North Pacific mode and a tropical ocean-atmosphere coupled mode, the ENSO mode. The NP and ENSO modes exhibit contrasting spatial and temporal characteristics. For the NP mode, the atmospheric variation leads changes in SST, while for the ENSO mode the opposite is true. The NP mode displays a persistence barrier during AUG-SEP whereas the ENSO mode has a MAR-APR persistence barrier. The upper-troposphere jet stream associated with the NP and ENSO modes intensifies, respectively, over the central North Pacific and the subtropical northeastern Pacific; consequently, the transient activities maximize in their corresponding jet exit regions. The significant simultaneous correlation between NP-GPH and ENSO-GPH time series becomes insignificant, by reducing the high-frequency variation. Our results suggest that the intrinsic coupled mode in the midlatitude North Pacific may be distinguished from the forced mode by remote ENSO, especially on the interannual time scale.

REFREENCE

An, S.-I., 2003: Conditional maximum covariance analysis and its application to the tropical Indian

Ocean SST and surface wind stress anomalies, *J. Climate*, **16**, 2932-2938.
Frankignoul, C., and K. Hasselmann, 1977: Stochastic climate models. Part II: Application to sea-surface temperature anomalies and thermocline variability. *Tellus*, **29**, 284-305.
Horel, J., and J. M. Wallace, 1981: Planetary scale atmospheric phenomena associated with the Southern Oscillation. *Mon. Wea. Rev.*, **109**, 813-829.
Kalnay, et al. 1996: The NCEP/NCAR 40-year reanalysis project. *Bull. Amer. Met. Soc.*, **77**, 437-471.
Reynolds, R. W., and T. M. Smith, 1994: Improved global sea surface temperature analysis using optimum interpolation. *J. Climate*, **7**, 929-948.
Simmons, A. J., J. M. Wallace, and G. W. Branstator, 1983: Barotropic Wave Propagation and Instability, and Atmospheric Teleconnection Patterns. *J. Atmos. Sci.*, **40**, 1363-1392.
Straus, D. M., and J. Shukla, 2002: Does ENSO force the PNA? *J. Climate*, **15**, 2340-2358.
Wallace, J. M., and D. S. Gutzler, 1981: Teleconnections in the geopotential height field during the Northern Hemisphere winter. *Mon. Wea. Rev.*, **109**, 784-812.
Wallace, J. M., C. Smith, and C. S. Bretherton, 1992: Singular value decomposition of wintertime sea surface temperature and 500-mb height anomalies. *J. Climate*, **5**, 561-576.
Zhang, Y., J. M. Wallace, and N. Iwasaka, 1996: Is climate variability over the North Pacific a linear response to ENSO? *J. Climate*, **9**, 1468-1478.

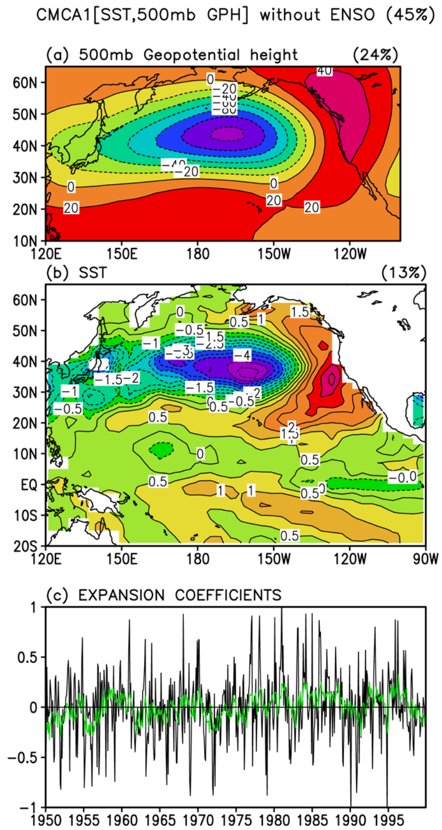

Fig. 1 Spatial patters of the first CMCA mode associated with (a) 500mb GPHand (b) SST. The corresponding expansion coefficients associated with 500mb GPH (black curves) and SST (greencurves) are shown in (c). Nino-3 index was used as the secondary predictor.

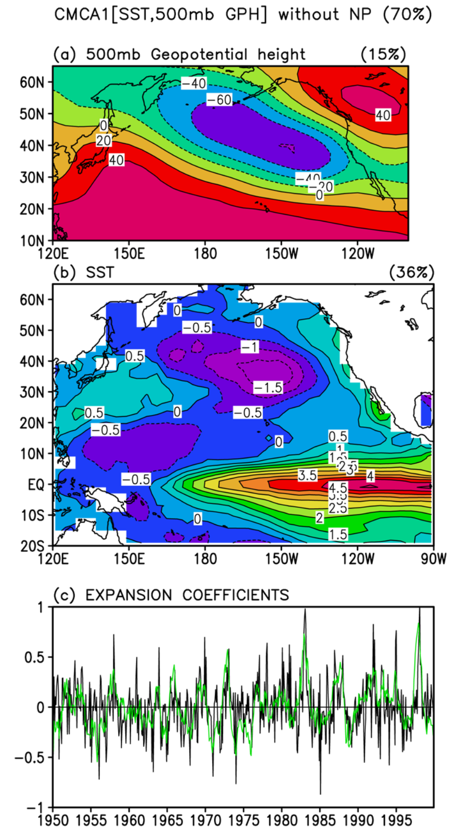

Fig. 2 As in Fig. 1 but for the ENSO mode. The expansion coefficients of NP mode was used as the secondary predictor.

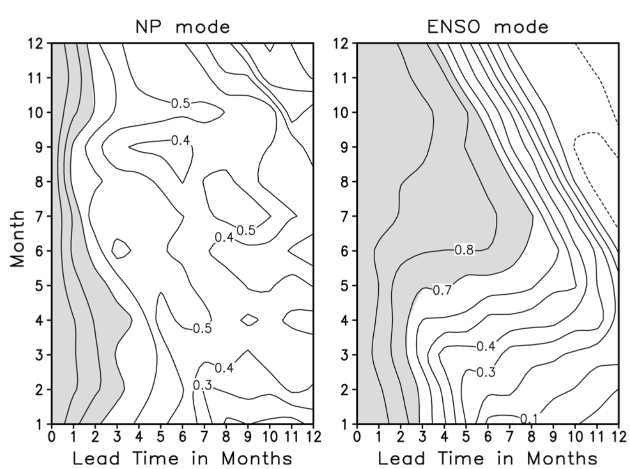

Fig. 3 Lag correlation of (a) NP-SST time series and (b) ENSO-SST time series s a functionof start month and lead-time.

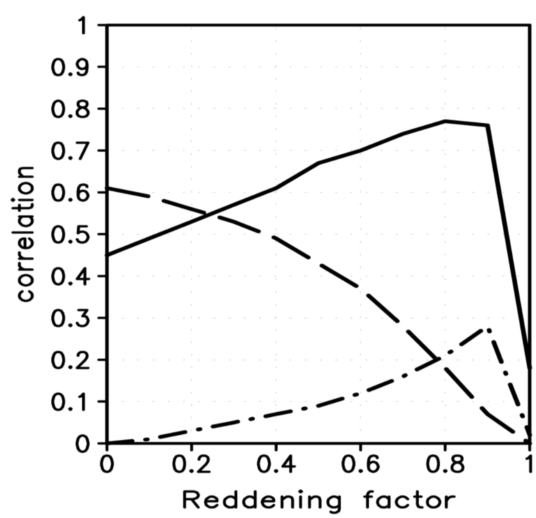

Fig. 4 Correlations between the reddened NP-GPH time series and NP-SST time series as a function of the reddening factor (solid line). Dashed (dash-dotted) line indicates correlations between the reddened NP-GPH time series and ENSO-GPH time series (correlations between the reddened ENSO-GPH time series and NP-SST time series).